Microchimica Acta (2020) 187: 403
https://doi.org/10.1007/s00604-020-04363-y

ORIGINAL PAPER

Solid-state ion recognition strategy using 2D hexagonal mesophase silica monolithic platform: a smart two-in-one approach for rapid and selective sensing of Cd^{2+} and Hg^{2+} ions

Aswanidevi Kongasseri[1] · Naveen Kumar Sompalli[1] · Varad A. Modak[1] · Ankita Mohanty[1] · Sivaraman Nagarajan[2] · C.V.S. Brahmananda Rao[2] · Prabhakaran Deivasigamani[1] · Akhila Maheswari Mohan[1]

Received: 7 February 2020 / Accepted: 31 May 2020 / Published online: 24 June 2020

Abstract

The possibility of a multifunctional and reversible solid-state colorimetric sensor is described for the identification and quantification of ultra-trace Cd^{2+} and Hg^{2+} ions, using a honeycomb-structured mesoporous silica monolith conjoined with an indigenous chromoionophoric probe, i.e., 4-hexyl-6-((5-mercapto-1,3,4-thiadiazol-2-yl)diazenyl)benzene-1,3-diol (HMTAR). The amphiphilic probe is characterized using NMR, FT-IR, HR-MS, and CHNS elemental analysis. The structural and surface properties of the monolithic template have been characterized using p-XRD, XPS, TEM-SAED, SEM-EDAX, FT-IR, TG-DTA, and N_2 isotherm analysis. The unique structural features and distinct analytical properties of the solid-state sensor proffer a strong response in selectively signaling the target analytes. The probe (HMTAR) exhibits a 1:1 stoichiometric binding ratio with the target ions (Cd^{2+} & Hg^{2+}), with a visual color change from pale orange to dark red for Cd^{2+} (525 nm, λ_{max}), and to purple for Hg^{2+} (530 nm, λ_{max}), respectively, in the pH range 7.0–8.0. The influence of various analytical criteria such as pH, temperature, response kinetics, critical probe concentration, sensor quantity, matrix tolerance, linear response range, reusability, the limit of detection (LOD), and quantification (LOQ) has been investigated to validate the sensor performance. The proposed method displays a linear signal response in the concentration range 5–100 μg/L, with a LOD value of 2.67 and 2.90 μg/L, for Cd^{2+} and Hg^{2+}, respectively. The real-world efficacy of the sensor material has been tested with real and synthetic water samples with a significant recovery value of ≥ 99.2%, to authenticate its data reliability and reproducibility (RSD ≤ 3.53%).

Keywords Silica monolith · Mesoporous · Chromoionophore · Optical sensor · Cadmium · Mercury

Introduction

Considering the potential toxicological impact of cadmium and mercury, due to their wide range of industrial and consumer applications, there is an urgent need for their detection and extraction owing to their rampant proliferation in the environment [1–3]. Taking into account their environmental risk factors, deciding on the appropriate methodology will help in the effective treatment of any adverse fallout from various environmental and industrial sources. Hence, the current trend is to develop sensitive, selective, and robust sensing methods that can provide reliable results for ultra-trace levels of analytes present in slightly adverse conditions [4–6]. To date, there are mostly reports on the singular detection and determination of Cd^{2+} and Hg^{2+} ions through liquid-based colorimetric and fluorimetric analysis using organic solvent compatible supramolecular ligands that are non-reusable and non-benign [7, 8]. Moreover, the organic solvent-based analytical

K. Aswanidevi and S. Naveen Kumar contributed equally to this work.

Electronic supplementary material The online version of this article (https://doi.org/10.1007/s00604-020-04363-y) contains supplementary material, which is available to authorized users.

✉ Prabhakaran Deivasigamani
prabhakarswordy@gmail.com

✉ Akhila Maheswari Mohan
akhila.maheswari@vit.ac.in

[1] Department of Chemistry, School of Advanced Science (SAS), Vellore Institute of Technology (VIT), Vellore, Tamil Nadu 632014, India

[2] Homi Bhabha National Institute (HBNI), Indira Gandhi Centre for Atomic Research (IGCAR), Kalpakkam, Tamil Nadu 603102, India

methods are non-compatible for the direct analysis of metal ions in environmental samples. Indeed, there are limited literature reports on solid-state sensing, where the matrix or the template varies from nanoparticles to metal-organic frameworks (MOFs). Li et al. have reported on the utility of bimetallic Ag-Cu nanoparticles (NPs) for the determination of Hg^{2+} ions [9]. Similarly, Guo et al. reported the colorimetric sensing of Cd^{2+} ions using Au NPs [10]. Butwong et al. reported on colorimetric test strips by incorporating Ag NPs doped CdS quantum dots in chitosan-coated cellulose material for the determination of Hg^{2+} ions [11]. Likewise, Patir et al. studied carbon dots for the detection of Hg^{2+} by exploiting their photoluminescence property [12]. However, the major disadvantage with these approaches lies in the concrete adhesion toward fluorescence and phosphorescence properties, which lacks its utility as a naked-eye probing material. Moreover, the use of NPs could potentially lead to nanotoxicity and non-recoverable issues, despite their sensitivity factor. Kim et al. reviewed the use of various colorimetric and fluorimetric detection strategies for Cd^{2+} and Hg^{2+} ions, where they highlight not only on the ion selectivity issues but also on the generation of secondary pollutants (by organic solvents), thereby making the literature methods less effective, for futuristic approach [13]. Further, it is well-known that instrumental techniques, such as GF-AAS, ICP-MS, ICP-OES, IC, and AFS, can be an efficient tool for the detection and determination of heavy metal ions. However, these techniques remain unaffordable to the majority of the scientific communities in most of the developing and underdeveloped countries. Furthermore, these techniques are commonly associated with chemical, matrix, and spectral interferences that could hinder their ion sensitivity and selectivity features, thereby necessitating a sample pre-treatment procedure. Thus, the advantages of instrumental techniques are outweighed by the cost, complexity, inaccessibility, and portability factors [14].

In recent years, the focus on developing benign ion-sensing methods by using simple, smart, and real-time approaches is on a steady rise for the monitoring of potentially hazardous substances. Thus, keeping in mind the progressive nature of the scientific temper, researchers are now concentrating on smarter techniques, newer materials, and innovative assemblies [15–31]. In this line, structurally engineered materials are an emerging trend that is making significant process in addressing the issues related to metal ion sensing.

A variety of innovative materials in the form of nanofilms, polymers, and inorganic frameworks have been experimented to arrive at an intuitive solution [32–36]. However, the significant challenges associated with the fabrication of a solid-state method are its cost-effectiveness, design accuracy, metal ion binding affinity, and structural properties of the probe. Several geometrical properties influence the behavior and topologies of the final product either through electrical or spatial interactions. However, with the development of monolithic entities, the options and methodologies that are possible to assemble have multiplied by leaps and bounds [37–40]. Silica-based porous monolithic structures are one of the widely attractive materials in the field of material science owing to its unique structural properties and also growing range of applications. The intact texture of these monolithic designs with a highly sequential porous gradient that is distributed uniformly across the material makes it an essential functional scaffold with potential applications in optical ion sensing and adsorption chemistry [41–43]. Indubitably, the active tuning of the shape and size of the monolithic pores is a critical factor in regulating the sensitivity of any monitoring system. Thus, the monolithic assemblies can allow solid-state naked-eye sensing of heavy metal ions even at ultra-trace levels through specific anchoring of probe ligands of specific metal ion affinity.

In the present work, we construe the synthesis, structural modification, and analytical characteristics of a two-way solid-state colorimetric method for the detection and determination of Hg^{2+} and Cd^{2+} ions, by using a probe-hosted honeycomb-structured mesoporous silica monolithic template. The uniqueness of this work is the first of its kind attempt on the twin utility of a solid-state monolithic sensory material, which not only acts as a naked-eye colorimetric method for the detection of ultra-trace toxic Hg^{2+} and Cd^{2+} ions but also as an ion concentrator. Besides, the current method is durable and reusable for numerous cycles with excellent data reliability. The proposed solid-state colorimetric-based ion-sensing approach is envisaged to open new avenues for potable and smart diagnostic tools that can be handled even by the non-technical populace, without tedious sample pre-treatment procedures.

Materials and methods

Chemicals and instrumentations

All the chemicals and reagents used for the synthesis of monolithic template and probe molecule are from Sigma-Aldrich and are of ≥ 99% purity. For the silica monolith synthesis, chemicals such as tetraethyl orthosilicate (TEOS, silica precursor), 1,3-diisopropyl benzene (DiPB, porogen), and Pluronic F127 (F127, structure-directing agent) are used. For the synthesis of probe molecule (HMTAR), i.e., 4-hexyl-6-((5-mercapto-1,3,4-thiadiazol-2-yl)diazenyl)benzene-1,3-diol, chemicals such as 2-amino-5-mercapto-1,3,4-thiadiazole, and 4-hexylresorcinol are used as reactants. The probe molecule (HMTAR) synthesis and its characterization are discussed in the Electronic Supporting Material. For all the ion-sensing and interference studies, AAS grade standard metal ion solutions (1000 ppm) are employed throughout the experiment. For pH adjustments, a series of 0.2 M buffers,

namely, $ClCH_2COOH$-HCl (pH 1–3), CH_3COONa-CH_3COOH (pH 4–6), MOPS-NaOH (pH 7–9), and CHES-NaOH (pH 10–11), are used.

The wide-angle and low-angle X-ray diffraction pattern for the synthesized silica monolithic material has been analyzed using a powder X-ray diffractometer (p-XRD, D8 Advance Bruker). The monolithic silica framework has been visualized using a high-resolution transmission electron microscope (HR-TEM, Tecnai, G2 20 Twin) and also using a field emission scanning electron microscope (FE-SEM, Hitachi S-4800). The surface area of the monolithic template and the resulting sensor materials are monitored by N_2 adsorption-desorption isotherm and calculated by the BET (Brunauer-Emmett-Teller) method. Likewise, the pore size distribution of the monolithic materials is evaluated by BJH (Barrett-Joyner-Halenda) method, using a Quantachrome instrument (Autosorb iQ) fitted with an automated gas sorption analyzer, coupled with Quantachrome ASiQwin™ software. For analyzing the elemental composition and oxidation state of the monolith sensors, an X-ray photoelectron spectrometer (XPS, PHI 5000 VersaProb-II), with a monochromatic Al Kα radiation, has been deployed. The functional group characterization of the probe molecule and the monolith framework is carried out using a Fourier transform infrared spectrophotometer (FT-IR, Thermo Scientific, Nicolet iS10). The thermal stability of the monolithic template and ion sensor is monitored using a thermogravimetric analyzer (TGA, Seiko, SII 7200), at a temperature ramp of 15 °C/min. The probe ligand is characterized using a 400 MHz NMR spectrometer (Bruker, AVANCE NEO), HR-MS (Waters, Xevo G2-XS QToF), and CHNS analyzer (Elementar Vario, Micro Select EL). The metal ion quantification studies are recorded using a UV-visible diffuse reflectance spectrophotometer (UV-Vis-DRS, Jasco V670). The quantification of the target metal ion concentrations, along with the matrix constituents present in real water samples, is carried out using ICP-MS (Agilent 7900). The temperature-controlled calcination of the silica monoliths is performed using a programmable muffle furnace (Nabertherm B10-LT5/11).

Synthesis of silica monolithic templates

For the synthesis of mesoporous silica monoliths, a 1.15 g of F127 is dissolved in 5.0 mL of 0.3 M HCl, which is stirred for 0.5 h, to attain a homogeneous solution. To this solution, a 0.5 mL of DiPB is added, and after 0.5 h of stirring, a 4.0 g of TEOS is added for the hydrolysis reaction. The mixture is stirred continuously for the formation of a sol, which is left undisturbed, resulting in the gelation process within 2 h. The wet gel is allowed to age for 24 h at 40 °C, and the solvents are allowed to evaporate at a steady state in order to avoid the rupture of the mesoporous network [43]. The solid gel is treated with 0.1 M of NH_4OH to remove the surfactant present in the monolith. Finally, it is calcined at 450 °C for 5 h, through a temperature ramping of 1 °C/min, to remove all the organic contents that are present in the monolith framework, to give a highly ordered mesoporous monolithic silica framework.

Growth mechanism of silica monolith

A sequence of the sol-gelation process initiates the structural growth of silica monolith by first hydrolyzing the silica precursor (TEOS) to Si-OH in the presence of HCl/H_2O at a defined solution pH. This is followed by the formation of silicate oligomers (Si-O-Si) through a temperature-controlled condensation process [42–45]. Henceforth, the silicate oligomers are treated with a non-ionic tri-block copolymer (Pluronic F127, $EO_{100}PO_{65}EO_{100}$), which acts as the structure-directing agent (SDA) that results in the nucleation and growth of the finely dispersed phase of silica oligomers into a 2D hexagonally packed condensed array in the presence of a non-polar porogenic solvent, i.e., 1,3-diisopropyl benzene (DiPB). The process follows a further formation/occurrence of a co-continuous domain structure as a result of the secondary binodal decomposition. During the sol-gel transition state, both the domain coarsening and structure freezing processes will be competitively visible, where the dominant one at the final stage determines the gel morphology. The pore structure has been tailored by aging, followed by the solvent exchange process. The meso-/microporous realm of the silica material filled with SDA is removed by a temperature-controlled calcination process that eventually results in the formation of a crack-free silica monolith network. The additional details in tailoring the growth of a silica monolith with specific structural features are provided in the Electronic Supplementary Material.

Fabrication of solid-state colorimetric monolithic sensor

The solid-state sensor is fabricated through the physical impregnation of the probe ligand (HMTAR) on to the silica monolith, through direct immobilization process. The main advantage of this process is that it effectively utilizes the silica monolith adsorption chemistry, thus resulting in high ion sensitivity down to ppb concentration. To intercalate the probe on the monolithic template, a known concentration of the probe is dissolved in ethanol and loaded onto the silica monolith (0.5 g) through continuous equilibration process. The solvent is removed using a rota evaporator, and the probe loading process is continued until the attainment of probe adsorption saturation on the monolithic template. After attaining the threshold level of loading, the monolithic sensor material is washed with deionized water and dried at 40 °C for 6 h. The monolith sensors are ground to a fine powder for the colorimetric sensing of Hg^{2+} and Cd^{2+}. The best ion-sensing results

are obtained with probe concentrations of 0.15 and 0.2 mmol/g, for Hg^{2+} and Cd^{2+}, respectively.

The amount of ligand loaded into the material is calculated using the equation:

$$A_t = \frac{(Po-Pt)\ V}{M}\ (\mathrm{mmol/g})$$

where, A_t is the amount of ligand adsorbed onto the monolith, at a time (t); V is the overall solution volume; M is the quantity of the monolithic template; and P_o and P_t correspond to the initial and threshold probe concentrations, respectively.

Colorimetric sensing of cadmium and mercury ions

The solid-state colorimetric detection and determination of Cd^{2+} and Hg^{2+} ions are carried out by equilibrating a small quantity (3.0–4.0 mg) of the sensor material with a 20 mL of an aqueous solution comprising of respective buffers along with individual Hg^{2+} and Cd^{2+} of varying concentrations (0.1–300 μg/L). The sensor materials are equilibrated with the metal ion solutions for a specific time and are filtered using a cellulose nitrate membrane filter (25 mm diameter, 0.45 μm pore size, Millipore). The resulting metal ion concentration proportionate color response is compared with the blank sensor, and their relative absorbance is measured by UV-Vis-DRS, for quantitative studies. All the analytical studies for sensing applications are subjected to triplicate analysis, with an observed relative standard deviation (RSD) value of ≤ 2.70%.

Result and discussion

Characterization of bare and probe-hosted silica monolith

The HR-SEM images of the mesoporous silica monolith templates prepared using F127 as the tri-block copolymer are depicted in Fig. 1(a–c). The SEM images reveal the existence of a topologically ordered arrangement of Si-O-Si linkage with a continuous porous network that travels uniformly across the monolith. The rough surface morphology observed for the synthesized silica monolithic template is suitable for host-guest interaction through adsorption chemistry. The porous topology unveils the effective sorption of the probe molecules, thereby creating a well-defined platform for the substrate-probe interaction. The HR-SEM images reveal the existence of a macroporous network with mesoporous channels for the silica monoliths. The porous nature of the monolithic framework enhances the metal ion diffusion on the probe anchored pore channels by acting as nanocarriers, thereby proving to be a promising candidate for ion-sensing applications. The pore size is tailor-made by varying the calcination temperature, which further highlights that the reaction conditions are very crucial in tuning the surface properties of the monolith.

The HR-TEM images of the synthesized mesoporous monolith template are depicted in Fig. 1 (d–f). The cross-sectional patterns reveal a highly ordered 2D hexagonal mesophase with regularly arranged honeycomb pores. The structural pattern and surface texture of the silica monolith are engineered through the appropriate structure-directing agents (SDAs), synonymously defined as the mesoscopic texturing agents. In the case of synthesized silica monoliths, the presence of multilevel porous architectures can be attributed to the choice of F127 (with appropriate concentration) as SDA, which is a tri-block copolymer with a hydrophobic core (PPO) and a hydrophilic corona (PEO) that modulates the anatomy of the monolith. The choice of the synthesis route strictly determines the nature of the intergrown mesostructure phases. The existence of a hexagonal mesophase and the presence of rough and wedged monolithic surface provide excellent physical phenomena in terms of adsorption properties. The d-spacing values are calculated using a fast Fourier transform (FFT) pattern, and the results are in correlation with the data obtained from low-angle XRD. The pore volume is calculated to be 3.27 nm, which matches with the pore volume data obtained from the BJH plot, using N_2 adsorption isotherm. The chemical composition of the synthesized monoliths has been analyzed by EDAX, which reveals that the silica monolith is purely composed of Si-O-Si network, which is further supported by elemental mapping analysis, as depicted in Fig. 1 (g, h, and i), respectively. The results also confirm the effective calcination of the silica monoliths, thereby ensuring the uniform arrangement of pores without any blockage from the SDAs and other impurities. The amorphous nature of the silica monoliths has been confirmed by SAED, which reveals the absence of any bright spots of diffraction patterns, as shown in the inset **(**Fig. 1(i)**)**.

The low-angle XRD (Fig. 2a) exhibits prominent peaks (2θ) at 0.91°, 1.57°, and 1.80°, which redefines the mesoporosity of the cultured monolith material. The intense peak at 0.91° corresponds to the (1 0 0) reflection plane, which accentuated the mesoporous structural architecture with ordered through pores along (1 1 0) and (2 0 0) reflections at an angle (2θ) of 1.57° and 1.80°, respectively. Interestingly, the peak (2θ) at 0.91° remains unaffected even after ligand anchoring, thus indicating the presence of an unaltered mesoporous monolithic texture, with high structural integrity. However, the presence of broad (1 1 0) and (2 0 0) reflections after probe impregnation confirms the domiciliation of the probe molecules in the porous material network. However, a decline in the peak intensity of (1 1 0) and (2 0 0) reflections is noticed by increasing the ligand loading concentration, which further proves the active intercalation of the probe molecules into the mesoporous network. The d-spacing values for the

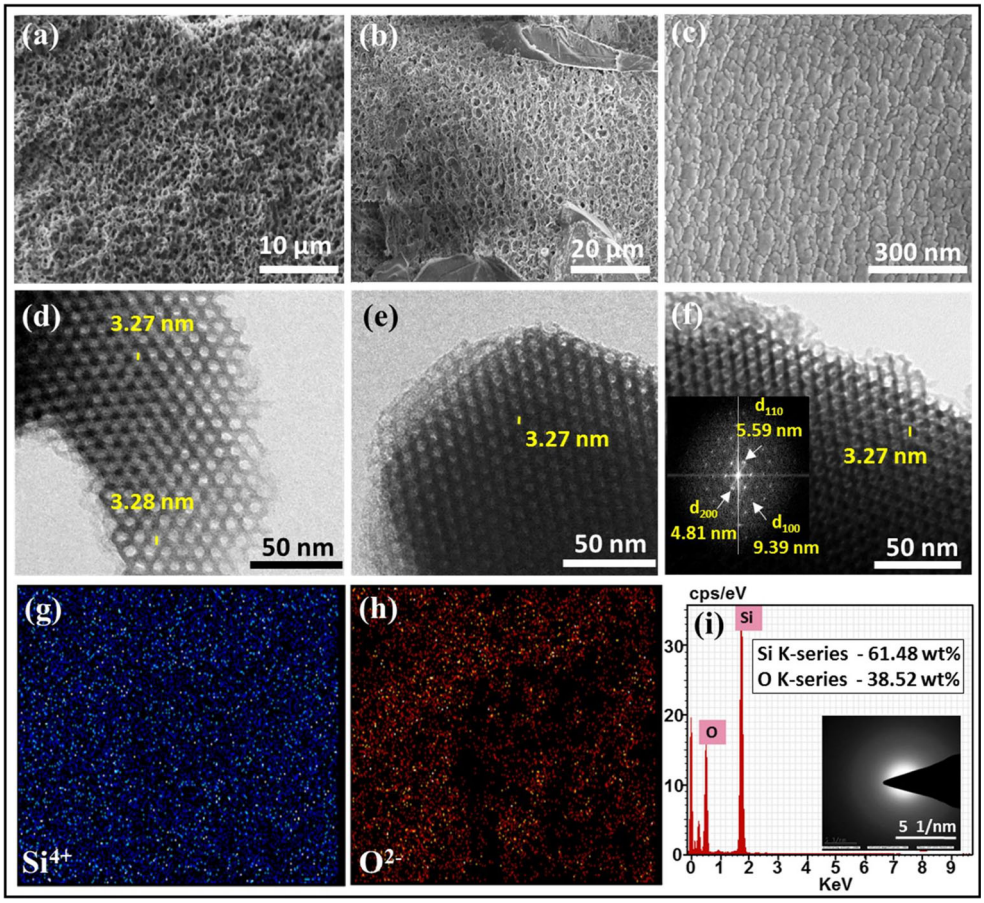

Fig. 1 (**a**–**c**) HR-SEM images, (**d**–**f**) HR-TEM images of varying resolutions, (**g** and **h**) elemental mapping, and (**i**) EDAX and SAED (inlet) of mesoporous silica monoliths prepared using F127 as SDA

prepared monolith material are calculated from the low-angle XRD pattern, which signifies a value of 4.81, 5.59, and 9.39 nm for (2 0 0), (1 1 0), and (1 0 0) reflection, respectively, thereby endorsing the hexagonal nature of the porous material

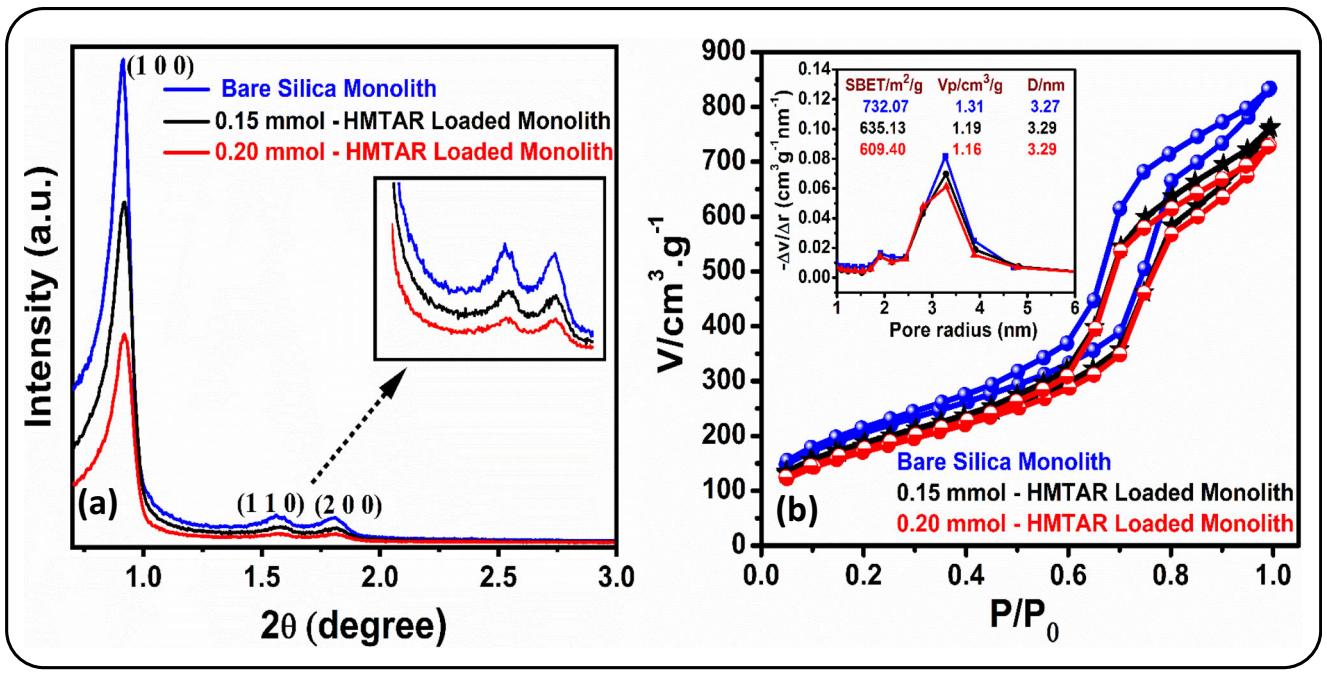

Fig. 2 **a** Low-angle XRD spectra and **b** N_2 adsorption-desorption isotherm and BJH pore size pattern (inset) for bare silica monolith, 0.15 mmol, and 0.20 mmol of HMTAR loaded silica monolithic template

by HR-TEM analysis. Similarly, the wide-angle p-XRD and FT-IR spectral analysis of Cd^{2+}/Hg^{2+} complexes of HMTAR anchored silica monolith to the bare silica monolith are discussed in the Electronic Supporting Material (Fig. S1(a, b)).

The surface area and pore dimensions of the bare and probe immobilized silica monolith are determined by N_2 isotherm analysis (at 77 K) using the BET and BJH method, respectively, and are depicted in Fig. 2b. The degassing of the sample (at 200 °C) before analysis helps in better resolution in visualizing the pores. The pore volume of the monolith has been calculated based on the quantity of N_2 molecules adsorbed at a relative pressure (P/P_0) of 0.999, with a temperature ramp of 10 °C/min. Based on BET surface area analysis, it is clear that the mesoporous silica exhibits an H1 hysteresis loop of type IV isotherm, thereby confirming the presence of a cylindrical pore arrangement of uniformity, with high pore volume and pore connectivity. The BET and the BJH plot implicate that the silica monolith prepared to possess a high surface area of 732.07 m^2/g, with a pore diameter and pore volume of 3.27 nm and 1.31 cm^3/g, respectively. However, upon 0.15 and 0.20 mmol of probe anchoring, a surface area value of 635.13 and 609.40 m^2/g is observed along with a slight shrinkage in the pore volume to 1.19 and 1.16 cm^3/g, respectively. This indicates the impregnation of the probe molecules across the porous silica monolithic template. It is also noticed that the shape of isotherm and the mode of hysteresis loop remained unaltered for both bare and ligand anchored silica monoliths, which further confirms the existence of a stable porous network, with well-defined pore channels.

The XPS spectra (both broad and short range) for the Cd^{2+}/Hg^{2+} complexes of HMTAR anchored silica monolith are depicted in Fig. 3 (a–d). The 2*p* spin-orbital coupling for the silica monolith has been deconvoluted, and the peaks at 103.1 and 102.5 eV correspond to the $2p_{1/2}$ state of Si-OH and $2p_{3/2}$ state of Si-O-Si linkage, respectively. The O 1 s peak is observed as a broad peak, which is deconvoluted to two peaks that correspond to the presence of two different oxygen moieties, i.e., the ionic oxygen (O^{2-}) present in Si-O-Si network at 531.2 eV and the surface Si-OH group at 533.3 eV. The complexation of the target metal ions, i.e., Hg^{2+} and Cd^{2+} with the probe molecules (inside the silica monolith), has been confirmed from the XPS spectral curve. It is observed that the Si 2*p* orbital peaks are overlapped with the Hg 4*f* spin-orbital peaks, which has been deconvoluted. The well-separated spin-orbit components ($\Delta = 4.0$ eV) of the Hg 4*f* region is obtained at 106.9 and 104.1 eV for Hg $4f_{5/2}$ and $4f_{7/2}$ orbital states, respectively, which confirm the divalent oxidation state of mercury ions in the HMTAR complex. In the case of cadmium ions, the peaks at 411.6 and 404.8 eV with a well-resolved spin-orbit component ($\Delta = 6.8$ eV) correspond to the Cd $3d_{3/2}$ and $3d_{5/2}$ orbital states, thereby confirming its divalent state. From the XPS data, the altered divalent oxidation states of the target metal ions (Cd^{2+}/Hg^{2+}) as HTMAR complexes within the silica monolith further confirm the formation of a charge-transfer complex. TG-DTA has studied the thermal stability and water-retaining capabilities of both bare and probe anchored silica monoliths, and the observations on the thermal analysis are discussed in the Electronic Supporting Material (Fig. S2).

Optimization of analytical parameters of the ion-sensor

To understand the optimum pH range for the sensor activity, a series of buffers ranging from pH 3.0 to 9.0 in 100 ppb of the target metal ion solutions are individually equilibrated with the sensor material, and the obtained response is shown in Fig. 4(a). From the plot, it is clear that the sensor signal response shows a gradual increase from pH 3.0 to 7.0 for Hg^{2+} ions, followed by a gradual fall beyond pH 7.0. In the case of Cd^{2+}, a similar trend has been noticed but with a maximum signal response at pH 8.0. It is also evident that the sensor system is not effective in acidic pH due to weak acidic property of the probe molecules that eventually reflected on the poor metal ion complexation with the ligand. This can also be explained with the protonation phenomena of the azo probe in acidic pH, where the protonated ligand less preferentially attacks the metal ion to form a charge-transfer complex. However, at pH > 9.0, the formation of stable anionic complexes of metal ions with hydroxyl ions makes the HMTAR-metal ion complexation less preferred. Thus, the solution pH of the sensor system plays a vital role in tuning the ion selectivity and sensitivity factor. The appropriate choice of solution pH makes the complexation process more facile and stable, thereby shifting the equilibrium toward metal ion complexation reaction.

Similarly, the amount of ligand loaded onto the monolith template is crucial, for which the colorimetric ion-sensing has been carried by coating various concentrations (0.05–0.3 mmol) of HMTAR, as shown in Fig. 4(b). From the results, it is clear that the use of 0.2 and 0.15 mmol of the probe provides the best signal response for Cd^{2+} and Hg^{2+} ions, respectively. This can be explained based on the effective stoichiometric complexation between the metal ion and the probe molecules. The portfolio of the sensor is maintained in such a manner that the complexation ratio calculated from Job's plot is strictly maintained so that the quantity of ligand's need for a definite metal ion concentration is fixed and UV-Vis-DRS measurements confirm the adopted paradigm. It is important to note that below the critical concentration of the anchored probe molecules, the metal ion complexation followed by the naked-eye colorimetric sensing is less effective. However, above the critical range, the excess ligand color hegemonies the charge transfer metal ion-ligand complex tincture, thereby reducing the sensitivity factor of the fabricated sensor array. Likewise, the influence of other analytical

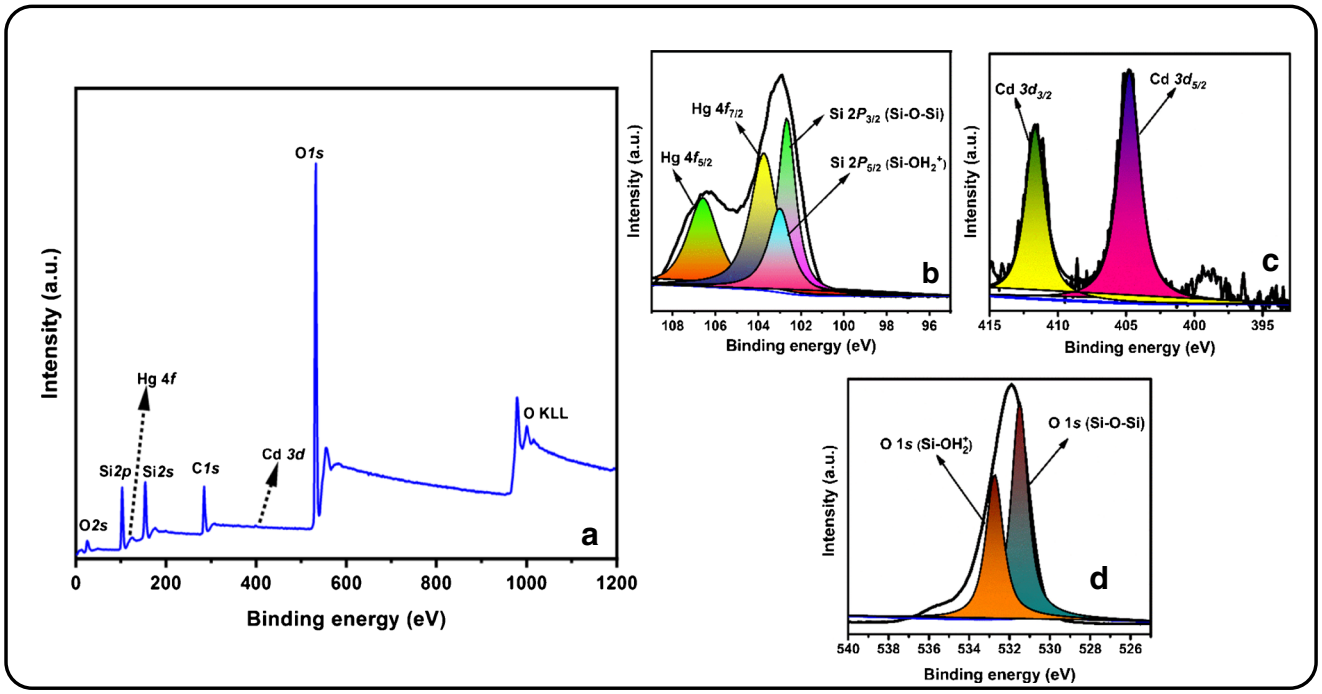

Fig. 3 (**a**) Wide-range XPS survey spectra for Hg^{2+} and Cd^{2+} complexes of HTMAR loaded silica monolith and (**b**–**d**) deconvoluted XPS spectra for *Si2p* and Hg^{2+}4f, Cd^{2+}3d, and O 1 s orbital states, respectively

parameters such as sensor quantity, kinetics of ion sensing, and solution temperature has been discussed in the Electronic Supporting Material (Fig. S3(a–d)). For the superlative performance of the fabricated sensor material, a sensor quantity material of 3.0 and 4.0 mg is necessitated, with response kinetics of 7 and 10 min for Hg^{2+} and Cd^{2+}, respectively, at 30 °C.

The ion selectivity paradigm for the monolithic sensor toward the target metal ions is investigated with a variety of common cations, anions, electrolytes, and surfactants, and their relative tolerance limit is tabulated in Table 1 and also depicted in Fig. 4(c). The ion recognition of the solid-state sensor shows excellent selectivity for the target metal ions and also shows high tolerance toward most of the commonly occurring anions and electrolytes. However, the cation interference studies reveal that the non-target metal ions such as Co^{2+}, Cu^{2+}, Ni^{2+}, and Pb^{2+} show intervention when their concentrations are > 10 times to that of the target ions, which are suitably eliminated using various masking agents. Hence, the addition of 0.45 mM citrate solution effectively suppresses the interference of Co^{2+} up to 40-fold of its concentration with respect to the target metal ions. For the interferences from Cu^{2+}, Ni^{2+}, and Pb^{2+}, the addition of 0.25 mM thiosulfate, 0.35 mM tartrate, and 34 μM EDTA solutions, respectively, ensures the elimination of their interference up to 100-folds of concentration with respect to the analyte ions. In addition, the ion-sensing efficiency of the sensor material has been tested amidst commonly used surfactants, which reveals outstanding selectivity for Hg^{2+} and Cd^{2+} ions, respectively, as depicted in Table 1. The incredible potentiality of the fabricated monolithic sensor can be ascribed to the chemical nature of the indigenously synthesized probe ligand (HMTAR) and the structurally designed monolithic template. The high ion selectivity associated with the solid-state sensor for the target analytes is attributed to the confined structural orientation of the amphiphilic probe molecules within the uniform porous network of the monolithic template that eventually results in specific geometrical complexation of the probe molecules with the target ions. Thus, the cumulative analytical results provide valuable information on the potential practical utility of the fabricated sensor for real-time applications.

The quantitative and qualitative ion-sensing efficiency of the two-in-one chemosensor has been assessed by using different concentrations of the target metal ion solutions (0–300 ppb), under appropriate experimental conditions, and their relative colorimetric and spectral responses are depicted in Fig. 5 (a and c). The absorbance for Hg^{2+} and Cd^{2+} complexes of the HMTAR sensor system is measured at (λ_{max}) 530 nm and 525 nm, respectively. The observed concentration proportionate color change is due to the formation of metal to ligand charge transfer complex between the d^{10} Hg^{2+} and Cd^{2+} electronic states with the HMTAR ligand moiety, as depicted in Fig. 5 (b and d). A linear signal response in the range of 5–100 ppb is observed for both sensors with a square correlation coefficient (r^2) of 0.999 and a slope of 0.005 and 0.0046 for Hg^{2+} and Cd^{2+}, respectively. The corresponding σ values

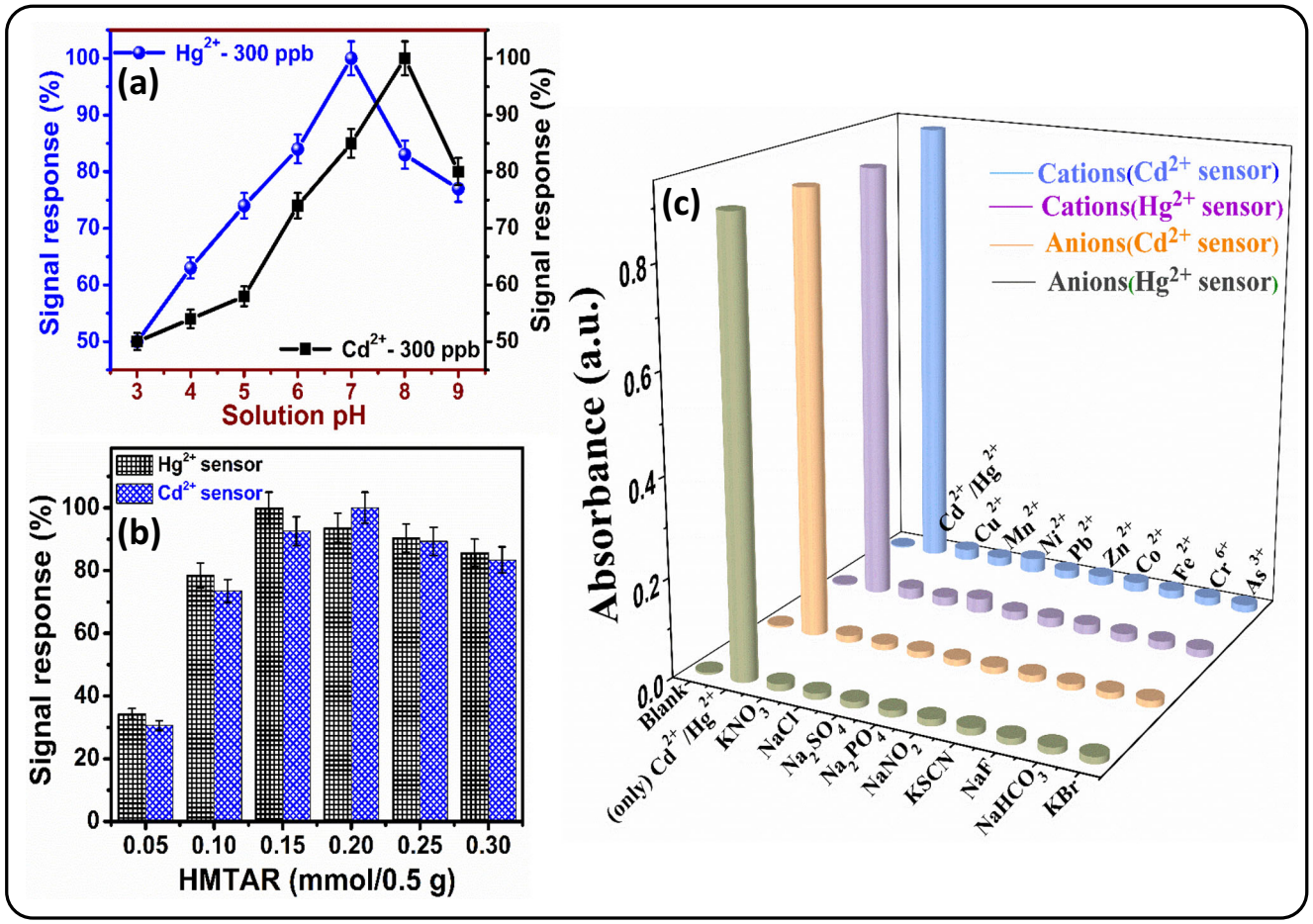

Fig. 4 Effect of (**a**) solution pH, (**b**) HMTAR loading concentration, and (**c**) selectivity studies for (100 ppb) Cd^{2+} & Hg^{2+} ion sensing in the presence of common cations and anions present in the water sample under optimized experimental conditions (RSD ≤ 2.55%)

Table 1 Tolerance limit for interfering foreign ions during target trace level (100 ppb) sensing of Hg^{2+} and Cd^{2+} ions

Common electrolytes		Common metal ions		Surfactants	
Electrolytes	Tolerance limit (ppm)	Cations	Tolerance limit (ppm)	Surfactants#	Tolerance limit (ppm)
NaCl	7300	Mn^{2+}	6.0	SDS	560
KNO_3	3600	$As^{3+/5+}$	9.5	DDAB	600
Na_2SO_4	2550	Pb^{2+}	3.7	CTAC	400
Na_3PO_4	6000	Ni^{2+}	2.5	CTAB	550
$NaNO_2$	400	Zn^{2+}	4.5	Triton X-100	600
Na_2SO_3	250	Cu^{2+}	3.0		
KSCN	150	Ca^{2+}	750		
CH_3COONa	4500	Mg^{2+}	640		
NaF	350	$Fe^{2+/3+}$	9.5		
$NaHCO_3$	1400	Co^{2+}	2.0		
$MgCO_3$	1100	Cr^{6+}	12		
KBr	850				

#*SDS* sodium dodecyl sulfate; *DDAB* dilauryldimethylammonium bromide; *CTAC* cetyltrimethylammonium chloride; *CTAB* cetyltrimethylammonium bromide

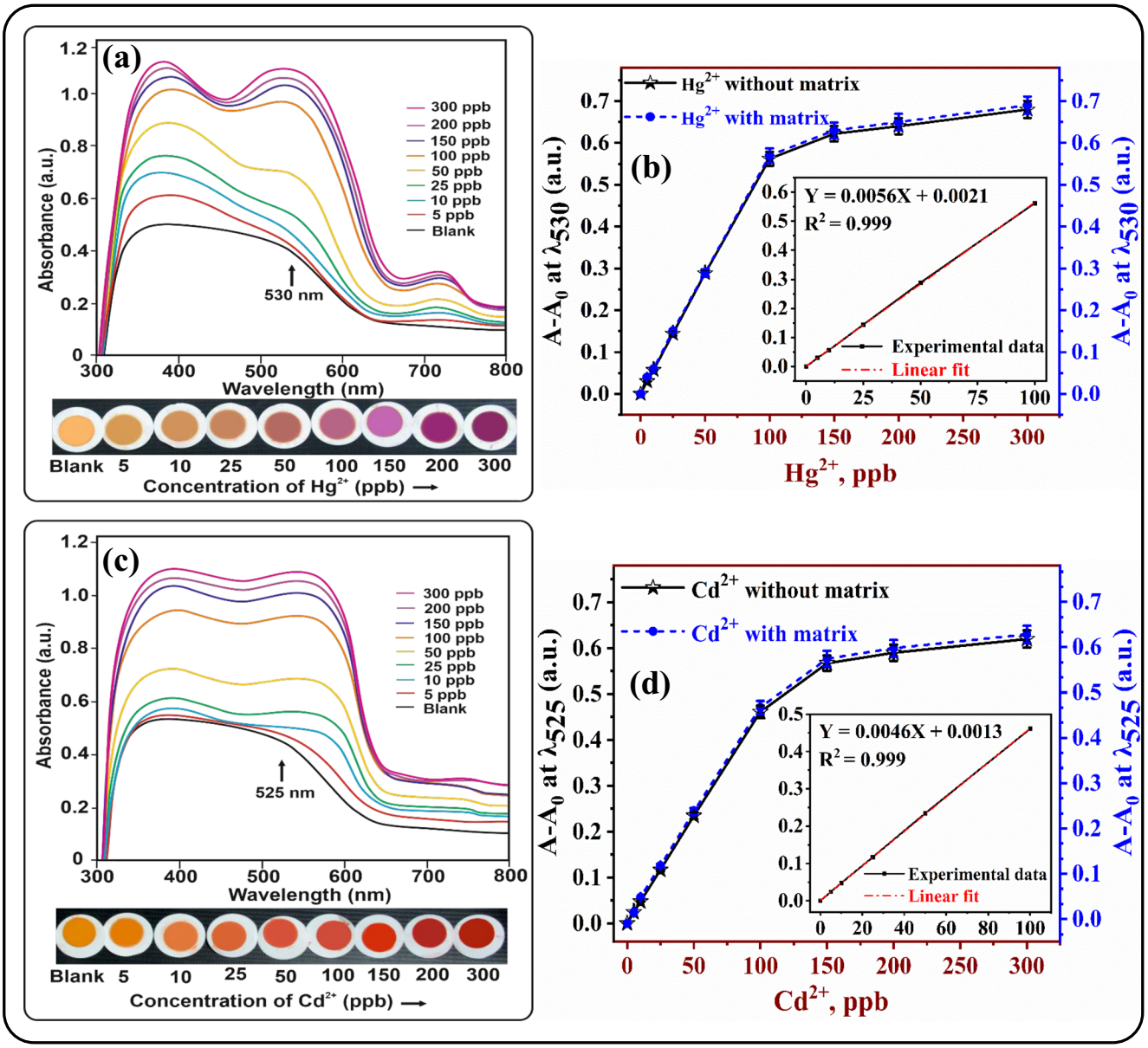

Fig. 5 (**a** and **c**) UV-Vis-DRS and naked-eye visual color transition for varying concentration of Hg^{2+} and Cd^{2+} ions. (**b** and **d**) Calibration plot (inlet plots signifies the linear response range) pertaining to Hg^{2+} and Cd^{2+} sensors (RSD ≤ 2.70%), respectively

are found to be 0.0048 and 0.0041. Accordingly, the LOD and LOQ for Hg^{2+} are 2.90 and 9.80 ppb, whereas for Cd^{2+}, it is 2.67 and 8.90 ppb, respectively. Based on the results, the analytical features of the proposed method are compared with literature reports, as shown in Table 2. The proposed solid-state sensor reveals excellent/superior LOD and LOQ values for the target metal ions when compared with methods based on MOF, liquid state, alumina-silica monolith, and L-B film sensor arrays [46–52]. Besides, the proposed sensor is a first of its kind solid-state material that possesses a two-in-one sensory behavior in efficiently detecting and determining two toxic heavy metal ions (Hg^{2+} and Cd^{2+}). The solution state binding stoichiometry between the metal ion and the synthesized HMTAR ligand has been studied using Job's method, for Hg^{2+} and Cd^{2+} sensing, respectively. Based on the continuous variation method, it is evident that both Cd^{2+}-HMTAR and Hg^{2+}-HMTAR follows a 1:1 complexation ratio, which is further supported by ^{1}H NMR titrations (as discussed in the Electronic Supporting Material, (Figs. S4–S8)). Similarly, the strong binding affinity (100-fold) of the target metal ions during complexation with the probe molecules (anchored in the porous silica monolith) in comparison with its liquid-state (organic solvent) has been discussed in the Electronic Supporting Material (Figs. S9 and S10). The proposed sensor material

Table 2 Comparison table reflecting the features of the proposed monolithic solid-state naked-eye Hg^{2+} and Cd^{2+} sensors with reference to the other literature reports

S. No.	Method	Materials or probes used	Linear response range (μM)	Limit of detection (μg/L)	Ref.
1	Au NPs-based liquid state fluorescence quenching method for detection of Hg^{2+} ions	Bovine serum albumin functionalized fluorescent Au NPs	0.10–2.5	0.02	[46]
2	Solid-state naked-eye detection of Hg^{2+} ions using MOFs	Zirconia-based MOFs (UiO-66) modified with dithizone probe	0.001–0.5	10.4	[47]
3	Solid-state colorimetric detection of Hg^{2+} ions using silica NPs	Mesoporous silica nanosphere particles modified with thio-Michler's ketone	0.003–0.05	0.45	[48]
4.	Solid-state colorimetric detection of Hg^{2+} ions using mesoporous silica and alumina-silica monolith materials	Mesoporous cubic *lm3m* alumina-silica monolith modified with diphenylcarbazide	0.005–0.5	8.10	[49]
5.	Liquid state colorimetric detection of Cd^{2+} ions using gold nanoparticles.	Gold nanoparticles modified with 4-amino-3-hydrazino-5-mercapto-1,2,4 triazole	0.06–0.48	6.10	[50]
6.	Solid-state colorimetric detection of Cd^{2+} using Langmuir-Blodgett (L-B) technique	L-B films assemblies with 4-n-dodecyl-6-(2-thiazolylazo) resorcinol	0.025–4.46	8.00	[51]
7.	Solid-state colorimetric detection of Cd^{2+} using mesoporous silica monolith materials	Mesoporous silica monolith modified with 4-tert-Octyl-4-((phenyl) diazenyl)phenol	0.01–0.5	0.33	[52]
8.	Mesoporous silica monolith based naked-eye detection of Hg^{2+} and Cd^{2+} ions	Mesoporous silica monolith modified with 4-hexyl-6-((5-mercapto-1,3,4-thiadiazol-2-yl)diazenyl)benzene-1,3-diol (HMTAR).	Cd^{2+} – 0.025–0.50 Hg^{2+}– 0.025–0.50	2.67 2.90	This work

exhibits excellent reusability character up to seven repeated cycles of reuse and also exhibits good durability even after storage for over a year. A detailed description of the reusability and durability character of the proposed solid-state sensor has been explained in the Electronic Supporting Material (Fig. S11). The stability of the proposed sensors has been tested over a wide range of solution temperatures and pH conditions, where the sensor material remains stable in the conditions of 10 °C ≤ T°C ≤ 85 °C and 1.0 ≤ pH ≤ 10.5. Interestingly, only under extreme acid stress conditions (pH ≤ 1.0), the silica monolith structural integrity is compromised in the form of a partial collapse of the mesopores and its wall thickness.

To accomplish the practical usability of the prepared HMTAR-silica monolith solid-state sensor, the Hg^{2+} and Cd^{2+} ion recognition protocol are tested using real water and synthetic samples, for the recovery and quantification of the target analytes from complex matrix environment. For this, water samples, namely, groundwater, lake water, river water, and a treated (domestic) wastewater, are collected in and around the Vellore district of Tamil Nadu, India. The samples are spiked with the target metal ions of varying concentrations and subjected to the ion-sensing process using the proposed monolithic solid-state sensor. The composition of the matrix constituents present in the water samples has been quantified by ICP-MS analysis, before the spiking of known quantities of Hg^{2+} and Cd^{2+} ions, as indicated in Table 3. The resulting analytical data using the sensor material has been cross-checked by ICP-MS analysis, to ascertain the data reliability and reproducibility. From the results, a recovery value of ~ 99% (RSD ≤ 3.53%) is observed from the spiked water samples, thereby validating the practical modality of the proposed sensor for real-time field screening.

Conclusion

A probe anchored (HMTAR) hexagonal array of honeycomb-structured mesoporous silica monolith has been used as a smart two-in-one solid-state chemosensor for the colorimetric detection and quantification of Cd^{2+} and Hg^{2+} ions, with a faster response time of ≤ 10 min. The superior sensor performance has been attributed to its surface and pore properties, with excellent ion selectivity due to the restrained spatial orientation of the probe molecules confined within the monolithic network that provides better

Table 3 Practical utility of the proposed sensor for the detection and determination of Hg^{2+} and Cd^{2+} from environmental and synthetic water samples

Sample Source	Composition (ppm)	Spiked Amount (ppb)		Recovered Amount (ppb), Hg^{2+} - Sensor	Recovered Amount (ppb), Cd^{2+} - Sensor
		Hg^{2+}	Cd^{2+}		
Groundwater	Ni^{2+}, Zn^{2+}, Cu^{2+}, Co^{2+}: ≤ 0.5	0	0	0	0
	Mn^{2+}, $Fe^{2+/3+}$: ≤ 1.9	10	10	$9.7^{a} \pm 1.5^{b}$	$9.6^{a} \pm 2.2^{b}$
	Mg^{2+}, Ca^{2+}, Na^{+}, K^{+}: ≤ 455	15	15	$14.8^{a} \pm 2.7^{b}$	$14.8^{a} \pm 3.1^{b}$
	F^{-}, NO_3^{2-}, PO_4^{3-}: ≤ 140	25	25	$24.9^{a} \pm 2.0^{b}$	$23.2^{a} \pm 1.7^{b}$
	Cl^{-}, CO_3^{2-}, HCO_3^{-}: ≤ 310	50	50	$49.5^{a} \pm 3.5^{b}$	$49.6^{a} \pm 2.9^{b}$
Lake Water	Ni^{2+}, Zn^{2+}, Cu^{2+}, Co^{2+}: ≤ 0.4	0	0	0	0
	Mn^{2+}, $Fe^{2+/3+}$: ≤ 1.5	10	10	$9.5^{a} \pm 1.3^{b}$	$9.8^{a} \pm 2.1^{b}$
	Mg^{2+}, Ca^{2+}, Na^{+}, K^{+}: ≤ 240	15	15	$14.2^{a} \pm 2.0^{b}$	$14.8^{a} \pm 1.5^{b}$
	F^{-}, Cl^{-}, NO_3^{2-}, PO_4^{3-} : ≤ 105	25	25	$23.7^{a} \pm 2.5^{b}$	$24.2^{a} \pm 3.0^{b}$
	CO_3^{2-}, HCO_3^{-}: ≤ 180	50	50	$48.5^{a} \pm 1.5^{b}$	$49.0^{a} \pm 2.5^{b}$
River Water	Ni^{2+}, Zn^{2+}, Cu^{2+}, Co^{2+}: ≤ 0.25	0	0	0	0
	Mn^{2+}, $Fe^{2+/3+}$: ≤ 1.3	10	10	$9.3^{a} \pm 1.7^{b}$	$9.4^{a} \pm 1.5^{b}$
	Mg^{2+}, Ca^{2+}, Na^{+}, K^{+}: ≤ 190	15	15	$14.5^{a} \pm 3.0^{b}$	$14.0^{a} \pm 3.0^{b}$
	F^{-}, Cl^{-}, NO_3^{2-}, PO_4^{3-} : ≤ 70	25	25	$24.3^{a} \pm 1.8^{b}$	$23.5^{a} \pm 2.0^{b}$
	CO_3^{2-}, HCO_3^{-}: ≤ 160	50	50	$47.6^{a} \pm 3.0^{b}$	$47.5^{a} \pm 2.5^{b}$
Treated Wastewater	Na^{+}, K^{+}, Ca^{2+}, Mg^{2+}: 280				
	Cl^{-}, NO_3^{2-}, PO_4^{3-}: ≤ 200	0	0	0	0
	CO_3^{2-}, HCO_3^{-}: ≤ 190	20	20	$20.3^{a} \pm 1.5^{b}$	$19.9^{a} \pm 1.9^{b}$

[a] Average of three measurements

[b] Standard deviation

accessibility to the probe reaction sites. The metal ion concentration proportionate sensor response is visualized from the initial pale orange to dark red and purple color transitions for Cd^{2+} and Hg^{2+} ions, respectively, due to the metal-ligand charge transfer process. The testing of sensor materials in various water samples reveals its data reliability and reproducibility properties, besides confirming its potential utility for both field screening and real-time analysis. However, the sensor requires careful handling when dealing with extreme environmental conditions such as high acidity that could potentially disintegrate the porous silica monolithic framework due to partial hydrolysis. Despite the above limitation, the solid-state sensor ensures excellent stability and reusability character. Moreover, the mesoporous silica monolith can be easily synthesized by adopting the standard procedures without the necessity for an expertized workforce. However, the proposed methodology can be transformed into a large-scale device fabrication, which is quite likely to happen shortly. In this aspect, the potential features of the proposed sensor design will promote the rational design of more superior devices for the monitoring of other toxic metal ions.

Acknowledgments The authors also acknowledge the instrumentation support from IISc, IIT (Madras & Delhi), BIT (Bengaluru), and VIT (Chennai Campus).

Funding information The authors acknowledge the financial support from SERB (Project No.SB/FT/CS-051/2014), IGCAR Kalpakkam

(IGCAR/M&MFCG/FChD/SCSS/01/2018/ W.O.No.VITV-01), and VIT-Vellore (Institute Seed Grant).

Compliance with ethical standards

Conflict of interest The authors declare that they have no competing of interests.

References

1. Tinkov AA, Gritsenko VA, Skalnaya MG, Cherkasov SV, Aaseth J, Skalny AV (2018) Gut as a target for cadmium toxicity. Environ Pollut 235:429–434. https://doi.org/10.1016/j.envpol.2017.12.114
2. Vardhan KH, Kumar PS, Panda RC (2019) A review on heavy metal pollution, toxicity and remedial measures: current trends and future perspectives. J Mol Liq 290:111197. https://doi.org/10.1016/j.molliq.2019.111197
3. Li P, Feng XB, Qiu GL, Shang LH, Li ZG (2009) Mercury pollution in Asia: a review of the contaminated sites. J Hazard Mater 168:591–601. https://doi.org/10.1016/j.jhazmat.2009.03.031
4. Clarke RP (2015) Rising-falling mercury pollution causing the rising-falling IQ of the Lynn-Flynn effect, as predicted by the antiinnatia theory of autism and IQ. Pers Individ Dif 82:46–51. https://doi.org/10.1016/j.paid.2015.02.039
5. Qin L, Hu Q, Li YY, Wang L, Shi XX, Shen H, Wu Y, Zhao JL (2018) The Cd(II) – citric acid coordination polymer as an efficient sensor for the metal ions and organic molecules. Polyhedron 156:161–164. https://doi.org/10.1016/j.poly.2018.09.037
6. Rai PK, Lee SS, Zhang M, Tsang YF, Kim KH (2019) Heavy metals in food crops: health risks, fate, mechanisms, and management. Environ Int 125:365–385. https://doi.org/10.1016/j.envint.2019.01.067
7. Upadhyay S, Singh A, Sinha R, Omer S, Negi K (2019) Colorimetric chemosensors for d-metal ions: a review in the past, present and future prospect. J Mol Struct 1193:89–102. https://doi.org/10.1016/j.molstruc.2019.05.007
8. De Acha N, Elosúa C, Corres JM, Arregui FJ (2019) Fluorescent sensors for the detection of heavy metal ions in aqueous media. Sensors 19:599. https://doi.org/10.3390/s19030599
9. Li S, Wei T, Tang M, Chai F, Qu F, Wang C (2018) Facile synthesis of bimetallic Ag-Cu nanoparticles for colorimetric detection of mercury ion and catalysis. Sensors Actuators B Chem 255:1471–1481. https://doi.org/10.1016/j.snb.2017.08.159
10. Guo Y, Zhang Y, Shao H, Wang Z, Wang X, Jiang X (2014) Label-free colorimetric detection of cadmium ions in rice samples using gold nanoparticles. Anal Chem 86:8530–8534. https://doi.org/10.1021/ac502461r
11. Butwong N, Kunthadong P, Soisungnoen P, Chotichayapong C, Srijaranai S, Luong JHT (2018) Silver-doped CdS quantum dots incorporated into chitosan-coated cellulose as a colorimetric paper test stripe for mercury. Microchim Acta 185. https://doi.org/10.1007/s00604-018-2671-3
12. Patir K, Gogoi SK (2018) Facile synthesis of photoluminescent graphitic carbon nitride quantum dots for Hg^{2+} detection and room temperature phosphorescence. ACS Sustain Chem Eng 6:1732–1743. https://doi.org/10.1021/acssuschemeng.7b03008
13. Kim HN, Ren WX, Kim JS, Yoon J (2012) Fluorescent and colorimetric sensors for detection of lead, cadmium, and mercury ions. Chem Soc Rev 41:3210–3244. https://doi.org/10.1039/c1cs15245a
14. Urek SK, Nina F, Turel M, Lobnik A (2013) Sensing heavy metals using mesoporous-based optical chemical sensors. J Nanomater 2013:501320. https://doi.org/10.1155/2013/501320
15. Basavarajappa PS, Seethya BNH, Ganganagappa N, Eshwaraswamy KB, Kakarla RR (2018) Enhanced photocatalytic activity and biosensing of gadolinium substituted $BiFeO_3$ nanoparticles. ChemistrySelect 3:9025–9033. https://doi.org/10.1002/slct.201801198
16. Yang L, Yi G, Hou Y, Cheng H, Luo X, Pavlostathis SG, Luo S, Wang A (2019) Building electrode with three-dimensional macroporous interface from biocompatible polypyrrole and conductive graphene nanosheets to achieve highly efficient microbial electrocatalysis. Biosens Bioelectron 141:111444. https://doi.org/10.1016/j.bios.2019.111444
17. Shetti NP, Malode SJ, Nayak DS, Naik RR, Kuchinad GT, Reddy KR, Shukla SS, Aminabhavi TM (2020) Hetero nanostructured iron oxide and bentonite clay composite assembly for the determination of an antiviral drug acyclovir. Microchem J 155:104727. https://doi.org/10.1016/j.microc.2020.104727
18. Hui X, Xuan X, Kim J, Park JY (2019) A highly flexible and selective dopamine sensor based on Pt-Au nanoparticle-modified laser-induced graphene. Electrochim Acta 328:135066. https://doi.org/10.1016/j.electacta.2019.135066
19. Bukkitgar SD, Shetti NP, Kulkarni RM, Reddy KR, Shukla SS, Saji VS, Aminabhavi TM (2019) Electro-catalytic behavior of Mg-doped ZnO nano-flakes for oxidation of anti-inflammatory drug. J Electrochem Soc 166:B3072–B3078. https://doi.org/10.1149/2.0131909jes
20. Bukkitgar SD, Shetti NP, Malladi RS, Reddy KR, Kalanur SS, Aminabhavi TM (2020) Novel ruthenium doped TiO_2/reduced graphene oxide hybrid as highly selective sensor for the determination of ambroxol. J Mol Liq 300:112368. https://doi.org/10.1016/j.molliq.2019.112368
21. Shetti NP, Nayak DS, Malode SJ, Kakarla RR, Shukla SS, Aminabhavi TM (2019) Sensors based on ruthenium-doped TiO_2 nanoparticles loaded into multi-walled carbon nanotubes for the detection of flufenamic acid and mefenamic acid. Anal Chim Acta 1051:58–72. https://doi.org/10.1016/j.aca.2018.11.041
22. Shetti NP, Bukkitgar SD, Reddy KR, Reddy CV, Aminabhavi TM (2019) Nanostructured titanium oxide hybrids-based electrochemical biosensors for healthcare applications. Colloids Surfaces B Biointerfaces 178:385–394. https://doi.org/10.1016/j.colsurfb.2019.03.013
23. Dakshayini BS, Reddy KR, Mishra A, Shetti NP, Malode SJ, Basu S, Naveen S, Raghu AV (2019) Role of conducting polymer and metal oxide-based hybrids for applications in ampereometric sensors and biosensors. Microchem J 147:7–24. https://doi.org/10.1016/j.microc.2019.02.061
24. Shetti NP, Malode SJ, Ilager D, Raghava Reddy K, Shukla SS, Aminabhavi TM (2019) A novel electrochemical sensor for detection of molinate using ZnO nanoparticles loaded carbon electrode. Electroanalysis 31:1040–1049. https://doi.org/10.1002/elan.201800775
25. Shetti NP, Nayak DS, Malode SJ, Reddy KR, Shukla SS, Aminabhavi TM (2019) Electrochemical behavior of flufenamic acid at amberlite XAD-4 resin and silver-doped titanium dioxide/amberlite XAD-4 resin modified carbon electrodes. Colloids Surfaces B Biointerfaces 177:407–415. https://doi.org/10.1016/j.colsurfb.2019.02.022
26. Shetti NP, Malode SJ, Nayak DS, Bagihalli GB, Kalanur SS, Malladi RS, Reddy CV, Aminabhavi TM, Reddy KR (2019) Fabrication of ZnO nanoparticles modified sensor for electrochemical oxidation of methdilazine. Appl Surf Sci 496:143656. https://doi.org/10.1016/j.apsusc.2019.143656
27. Kumar S, Bukkitgar SD, Singh S, Pratibha SV, Reddy KR, Shetti NP, Venkata Reddy C, Sadhu V, Naveen S (2019) Electrochemical sensors and biosensors based on graphene functionalized with metal oxide nanostructures for healthcare applications.

ChemistrySelect 4:5322–5337. https://doi.org/10.1002/slct.201803871
28. Chaiyo S, Apiluk A, Siangproh W, Chailapakul O (2016) High sensitivity and specificity simultaneous determination of lead, cadmium and copper using μpAD with dual electrochemical and colorimetric detection. Sensors Actuators B Chem 233:540–549. https://doi.org/10.1016/j.snb.2016.04.109
29. Huang R, Shao N, Hou L, Zhu X (2019) Fabrication of an efficient surface ion-imprinted polymer based on sandwich-like graphene oxide composite materials for fast and selective removal of lead ions. Colloids Surfaces A Physicochem Eng Asp 566:218–228. https://doi.org/10.1016/j.colsurfa.2019.01.011
30. Awual MR, Islam A, Hasan MM, Rahman MM, Asiri AM, Khaleque MA, Chanmiya Sheikh M (2019) Introducing an alternate conjugated material for enhanced lead(II) capturing from wastewater. J Clean Prod 224:920–929. https://doi.org/10.1016/j.jclepro.2019.03.241
31. Awual MR, Alharthi NH, Hasan MM, Karim MR, Islam A, Znad H, Hossain MA, Halim ME, Rahman MM, Khaleque MA (2017) Inorganic-organic based novel nano-conjugate material for effective cobalt(II) ions capturing from wastewater. Chem Eng J 324:130–139. https://doi.org/10.1016/j.cej.2017.05.026
32. Rodman DL, Pan H, Clavier CW, Feng X, Xue ZL (2005) Optical metal ion sensor based on diffusion followed by an immobilizing reaction. Quantitative analysis by a mesoporous monolith containing functional groups. Anal Chem 77:3231–3237. https://doi.org/10.1021/ac048305+
33. El-Safty SA, Prabhakaran D, Kiyozumi Y, Mizukami F (2008) Nanoscale membrane strips for benign sensing of Hg(II) ions: a route to commercial waste treatments. Adv Funct Mater 18:1739–1750. https://doi.org/10.1002/adfm.200800035
34. Shahat A, Hassan HMA, El-Shahat MF, El Shahawy O, Awual MR (2019) A ligand-anchored optical composite material for efficient vanadium(II) adsorption and detection in wastewater. New J Chem 43:10324–10335. https://doi.org/10.1039/c9nj01818b
35. Bustamante SE, Vallejos S, Pascual-Portal BS, Muñoz A, Mendia A, Rivas BL, García FC, García JM (2019) Polymer films containing chemically anchored diazonium salts with long-term stability as colorimetric sensors. J Hazard Mater 365:725–732. https://doi.org/10.1016/j.jhazmat.2018.11.066
36. Hassan HMA, Shahat A, Azzazy HME, El-aal RMA, El-Sayed WN, Elwahed AA, Awual MR (2020) A novel and potential chemical sensor for effective monitoring of Fe(II) ion in corrosion systems of water samples. Microchem J 154:104578. https://doi.org/10.1016/j.microc.2019.104578
37. Balaji T, El-Safty SA, Matsunaga H, Hanaoka T, Mizukami F (2006) Optical sensors based on nanostructured cage materials for the detection of toxic metal ions. Angew Chemie - Int Ed 45:7202–7208. https://doi.org/10.1002/anie.200602453
38. Elshehy EA, EL-Safty SA, Shenashen MA (2014) Reproducible design for the optical screening and sensing of Hg(II) ions. Chemosensors 2:219–234. https://doi.org/10.3390/chemosensors2040219
39. El-Safty SA, Shenashen MA, El-Safty SA (2012) Mercury-ion optical sensors. TrAC - Trends Anal Chem 38:98–115. https://doi.org/10.1016/j.trac.2012.05.002
40. El-Safty SA, Deivasigamani P, Ismail AA, Matsunaga H, Mizukami F (2007) Nanosensor design packages: a smart and compact development for metal ions sensing responses. Adv Funct Mater 17:3731–3745. https://doi.org/10.1002/adfm.200700447
41. Showkat AM, Zhang YP, Min SK, Gopalan AI, Reddy KR, Lee KP (2007) Analysis of heavy metal toxic ions by adsorption onto amino-functionalized ordered mesoporous silica. Bull Kor Chem Soc 28:1985–1992. https://doi.org/10.5012/bkcs.2007.28.11.1985
42. Awual MR (2017) Novel nanocomposite materials for efficient and selective mercury ions capturing from wastewater. Chem Eng J 307:456–465. https://doi.org/10.1016/j.cej.2016.08.108
43. Sompalli NK, Mohan AM, Rao CVSB, Nagarajan S, Deivasigamani P (2019) Tailor-made porous polymer and silica monolithic designs as probe anchoring templates for the solid-state naked eye sensing and preconcentration of hexavalent chromium. Sensors Actuators B Chem 298:126896. https://doi.org/10.1016/j.snb.2019.126896
44. Kakarla RR, Lee KP, Kim JY, Lee Y (2008) Self-assembly and graft polymerization route to monodispersed Fe_3O_4@SiO_2-polyaniline core-shell composite nanoparticles: physical properties. J Nanosci Nanotechnol 8:5632–5639. https://doi.org/10.1166/jnn.2008.209
45. Reddy KR, Lee KP, Gopalan AI, Kang HD (2007) Organosilane modified magnetite nanoparticles/poly(aniline-co-o/m-aminobenzenesulfonic acid) composites: synthesis and characterization. React Funct Polym 67:943–954. https://doi.org/10.1016/j.reactfunctpolym.2007.05.023
46. Chai F, Wang T, Li L, Liu H, Zhang L, Su Z, Wang C (2010) Fluorescent gold nanoprobes for the sensitive and selective detection for Hg^{2+}. Nanoscale Res Lett 5:1856–1860. https://doi.org/10.1007/s11671-010-9730-y
47. Shahat A, Hassan HMA, Azzazy HME (2013) Optical metal-organic framework sensor for selective discrimination of some toxic metal ions in water. Anal Chim Acta 793:90–98. https://doi.org/10.1016/j.aca.2013.07.012
48. Shahat A, Trupp S (2017) Sensitive, selective, and rapid method for optical recognition of ultra-traces level of Hg(II), Ag(I), Au(III), and Pd(II) in electronic wastes. Sensors Actuators B Chem 245:789–802. https://doi.org/10.1016/j.snb.2017.02.008
49. El-Safty SA, Shenashen MA (2013) Optical mesosensor for capturing of Fe(III) and Hg(II) ions from water and physiological fluids. Sensors Actuators B Chem 183:58–70. https://doi.org/10.1016/j.snb.2013.03.041
50. Wang AJ, Guo H, Zhang M, Zhou DL, Wang RZ, Feng JJ (2013) Sensitive and selective colorimetric detection of cadmium(II) using gold nanoparticles modified with 4-amino-3-hydrazino-5-mercapto-1,2,4-triazole. Microchim Acta 180:1051–1057. https://doi.org/10.1007/s00604-013-1030-7
51. Deivaigamani P, Yuehong M, Nanjo H, Matsunaga H (2007) Naked-eye cadmium sensor: using chromoionophore arrays of Langmuir-Blodgett molecular assemblies. Anal Chem 79:4056–4065. https://doi.org/10.1021/ac0623540
52. Awual MR, Khraisheh M, Alharthi NH, Luqman M, Islam A, Rezaul Karim M, Rahman MM, Khaleque MA (2018) Efficient detection and adsorption of cadmium(II) ions using innovative nano-composite materials. Chem Eng J 343:118–127. https://doi.org/10.1016/j.cej.2018.02.116